Eur. Phys. J. C 30, 183–195 (2003)
Digital Object Identifier (DOI) 10.1140/epjc/s2003-01260-y

THE EUROPEAN PHYSICAL JOURNAL C

An analysis of the inclusive decay $\Upsilon(1S) \to \eta' X$ and constraints on the η'-meson distribution amplitudes

A. Ali[1,a], A.Ya. Parkhomenko[2,b]

[1] Theory Division, CERN, 1211 Geneva 23, Switzerland
[2] Institut für Theoretische Physik, Universität Bern, 3012 Bern, Switzerland

Received: 7 May 2003 /
Published online: 11 August 2003 –

Abstract. We calculate the η'-meson energy spectrum in the decay $\Upsilon(1S) \to \eta' ggg \to \eta' X$ in leading-order perturbative QCD in the static quark limit for orthoquarkonium. Our principal result is the extraction of parameters of the $\eta' g^* g$ effective vertex function (EVF) involving a virtual and a real gluon from the available data on the hard part of the η'-meson energy spectrum. The perturbative-QCD based framework provides a good description of the available CLEO data, allowing one to constrain the lowest Gegenbauer coefficients $B_2^{(q)}$ and $B_2^{(g)}$ of the quark–antiquark and gluonic distribution amplitudes of the η'-meson. The resulting constraints are combined with the existing ones on these coefficients from an analysis of the η–γ and η'–γ transition form factors and the requirement of positivity of the EVF, yielding $B_2^{(q)}(\mu_0^2) = -0.008 \pm 0.054$ and $B_2^{(g)}(\mu_0^2) = 4.6 \pm 2.5$ for $\mu_0^2 = 2\,\mathrm{GeV}^2$. This significantly reduces the current uncertainty on these coefficients. The resulting EFV $F_{\eta' g^* g}(p^2, 0, m_{\eta'}^2)$, including the η'-meson mass effects, is presented.

1 Introduction

Experiments involving the production and decays of the η- and η'-mesons are consistent with the picture that the η-meson is largely an $SU(3)_\mathrm{F}$ flavor-octet state, but the η'-meson contains a significant amount of an $U(3)_\mathrm{F}$ flavor-singlet quark–antiquark ($\bar{q}q$) component in its wave-function [1–5]; in addition, the gluonic (gg) content of the η'-meson is substantial [6]. This implies that for processes involving gluons and the η'-meson, in particular in the decays of heavy mesons of current phenomenological interest, such as $b \to s g \eta'$ inducing the $B \to \eta' X_s$ decay [7–13] and the exclusive $B \to (\eta, \eta')(K, K^*)$ decays [14–21], but also the inclusive decay of the orthoquarkonium $\Upsilon(1S) \to ggg^*(g^* \to \eta' g) \to \eta' X$ [22], the effective η'–gluon–gluon vertex plays an important role. This effective vertex function (EFV) has to be known sufficiently well to undertake a quantitative analysis of the data involving the η'-meson. Calling this EFV $F_{\eta' g^* g^*}(p_1^2, p_2^2, m_{\eta'}^2)$, where p_1^2 and p_2^2 are the virtualities of the two gluons, the QCD anomaly provides the normalization of this vertex for on-shell gluons, $F_{\eta' gg}(0, 0, m_{\eta'}^2)$. When one or both of the gluons are virtual with relatively large virtuality, the effective $\eta' g^* g^{(*)}$ vertex can be calculated in perturbative QCD [23–26].

In this approach, the η'-meson wave-function is described in terms of two light-cone distribution amplitudes (LCDAs) involving the quark–antiquark $\phi_{\eta'}^{(q)}(x, Q^2)$ and the gluonic $\phi_{\eta'}^{(g)}(x, Q^2)$ components, where x is the scaled energy of one of the partons of the η'-meson and Q^2 is the typical hard scale in the vertex. These two components mix if the QCD evolution is taken into account. The leading-twist LCDAs of the η'-meson can be expressed as an infinite series of the Gegenbauer polynomials $C_n^{3/2}(x - \bar{x})$ (for the quark–antiquark) and $C_{n-1}^{5/2}(x - \bar{x})$ (for the gluonic) components [27–32]

$$\phi_{\eta'}^{(q)}(x, Q^2) = 6x\bar{x} \left[1 + \sum_{\text{even } n \geq 2} A_n(Q^2)\, C_n^{3/2}(x - \bar{x}) \right], \quad (1)$$

$$\phi_{\eta'}^{(g)}(x, Q^2) = x^2 \bar{x}^2 \sum_{\text{even } n \geq 2} B_n(Q^2)\, C_{n-1}^{5/2}(x - \bar{x}), \quad (2)$$

where $\bar{x} = 1 - x$, and the following notation is used for the Gegenbauer moments:

$$A_n(Q^2) = B_n^{(q)}(\mu_0^2) \left(\frac{\alpha_\mathrm{s}(\mu_0^2)}{\alpha_\mathrm{s}(Q^2)} \right)^{\gamma_+^n} + \rho_n^{(g)}\, B_n^{(g)}(\mu_0^2) \left(\frac{\alpha_\mathrm{s}(\mu_0^2)}{\alpha_\mathrm{s}(Q^2)} \right)^{\gamma_-^n}, \quad (3)$$

[a] On leave of absence from Deutsches Elektronen-Synchrotron DESY, Hamburg, FRG

[b] On leave of absence from Department of Theoretical Physics, Yaroslavl State University, Sovietskaya 14, 150000 Yaroslavl, Russia

$$B_n(Q^2) = \rho_n^{(q)}\, B_n^{(q)}(\mu_0^2)\left(\frac{\alpha_s(\mu_0^2)}{\alpha_s(Q^2)}\right)^{\gamma_+^n} + B_n^{(g)}(\mu_0^2)\left(\frac{\alpha_s(\mu_0^2)}{\alpha_s(Q^2)}\right)^{\gamma_-^n}. \quad (4)$$

The constrained parameters $\rho_n^{(q)}$, $\rho_n^{(g)}$, γ_+^n and γ_-^n are computable and can be found, for example, in Appendix A of [24]. Usually, one employs an approximate form for the η'-meson LCDAs in which only the first non-asymptotic terms in both the quark–antiquark and gluonic components are kept. Thus, in this approximation

$$\phi_{\eta'}^{(q)}(x,Q^2) = 6x\bar{x}\left[1 + 6(1-5x\bar{x})\, A_2(Q^2)\right],$$
$$\phi_{\eta'}^{(g)}(x,Q^2) = 5x^2\bar{x}^2\,(x-\bar{x})\, B_2(Q^2), \quad (5)$$

where the explicit forms for $C_2^{3/2}(x-\bar{x})$ and $C_1^{5/2}(x-\bar{x})$ have been used. The free parameters $B_2^{(q)}(\mu_0^2)$ and $B_2^{(g)}(\mu_0^2)$, which enter in $A_2(Q^2)$ and $B_2(Q^2)$, are not determined from first principles, and have to be modeled or extracted from a phenomenological analysis of the data. To that end, a fit of the CLEO and L3 data on the η–γ and η'–γ transition form factors for Q^2 larger than $2\,\mathrm{GeV}^2$ [33,34] was recently undertaken in [25], yielding

$$A_2(1\,\mathrm{GeV}^2) = -0.08 \pm 0.04,$$
$$B_2(1\,\mathrm{GeV}^2) = 9 \pm 12, \quad (6)$$

where the initial scale of the evolution is taken as $\mu_0^2 = 1\,\mathrm{GeV}^2$. Note that the coefficients $A_2(1\,\mathrm{GeV}^2)$ and $B_2(1\,\mathrm{GeV}^2)$ are strongly correlated. The estimates (6) can be translated in terms of the universal free parameters $B_2^{(q)}$ and $B_2^{(g)}$, yielding

$$B_2^{(q)}(1\,\mathrm{GeV}^2) = 0.02 \pm 0.17,$$
$$B_2^{(g)}(1\,\mathrm{GeV}^2) = 9.0 \pm 11.5. \quad (7)$$

The current determination of these coefficients, in particular $B_2^{(g)}$, is rather poor, leading to a huge uncertainty in the evaluation of the $\eta' g^* g^{(*)}$ vertex function $F_{\eta' g^* g^{(*)}}(p_1^2, p_2^2, m_{\eta'}^2)$.

In this paper, we undertake a perturbative-QCD based analysis of the recent data on the inclusive process $\Upsilon(1S) \to \eta' X$ in the large η'-meson energy region published recently by the CLEO collaboration [35], which is expected to be dominated by the process $\Upsilon(1S) \to \eta' ggg \to \eta' X$. Moreover, Chen and Kagan [22] have argued that the shape of the η'-meson energy spectrum in this decay is sensitive to the shape of the $F_{\eta' g^* g}(p^2, 0, m_{\eta'}^2)$ vertex function, involving the η'-meson, a real and a virtual gluons (see Fig. 1). This sensitivity has already been used by the CLEO collaboration [35] to rule out certain models for this vertex, with the CLEO analysis favoring a rapidly falling p^2-dependence of the vertex $F_{\eta' g^* g}(p^2, 0, m_{\eta'}^2)$, in line with the perturbative-QCD predictions [23,24]. Motivated by these observations, we undertake a quantitative analysis of the CLEO data to constrain the LCDAs involving the quark–antiquark and the gluonic components of the η'-meson. The results of this analysis are presented in terms of the coefficients $B_2^{(q)}(2\,\mathrm{GeV}^2)$ and $B_2^{(g)}(2\,\mathrm{GeV}^2)$, where we have taken the initial scale as $\mu_0^2 = m_{\eta'}^2 + p_0^2 = 2\,\mathrm{GeV}^2$, which corresponds to the minimum gluon virtuality $p_0^2 \simeq 1\,\mathrm{GeV}^2$. This analysis is then combined with an earlier analysis of the η–γ and η'–γ transition form factors [25] to further constrain the two parameters. As the physical interpretation of the function $F_{\eta' g^* g}(p^2, 0, m_{\eta'}^2)$ is that it represents a probability distribution, much the same way as the partonic distributions are in, for example, deep inelastic lepton scattering off nucleons, this function must remain positive definite in the entire p^2 range. The requirement of positive definiteness of the function $F_{\eta' g^* g}(p^2, 0, m_{\eta'}^2)$ provides additional constraints on the parameters $B_2^{(q)}(2\,\mathrm{GeV}^2)$ and $B_2^{(g)}(2\,\mathrm{GeV}^2)$, in particular on the latter. The combined analysis leads to the following correlated ranges for these coefficients:

$$B_2^{(q)}(2\,\mathrm{GeV}^2) = -0.008 \pm 0.054\ ,$$
$$B_2^{(g)}(2\,\mathrm{GeV}^2) = 4.6 \pm 2.5\ . \quad (8)$$

Finally, we use this information to calculate the $F_{\eta' g^* g}(p^2, 0, m_{\eta'}^2)$ vertex, including the η'-meson mass effects, relegating the detailed derivation to a subsequent paper [36].

This paper is organized as follows: In Sect. 2, we calculate the branching ratio for the process $\Upsilon(1S) \to ggg^*$ $(g^* \to \eta' g) \to \eta' X$ and the η'-meson energy spectrum in this decay. A numerical analysis of the CLEO data is carried out in Sect. 3, and the resulting constraints are combined with the analysis of the η'–γ transition form factor to determine the LCDAs of the η'-meson. Section 4 contains a brief summary. The expressions for the matrix element squared for the decay $\Upsilon(1S) \to ggg^*(g^* \to \eta' g)$ are displayed in the appendix.

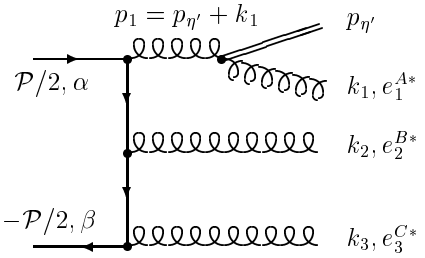

Fig. 1. A typical Feynman diagram describing the $\Upsilon(1S) \to ggg^*(g^* \to \eta' g) \to \eta' X$ decay. The directed solid line denotes the quark b and antiquark $\bar{b}$ of the Υ-meson and the double solid line denotes the η'-meson

2 Branching ratio and $E_{\eta'}$-distribution in the decay $\Upsilon(1S) \to \eta' ggg \to \eta' X$

Several processes contribute to the inclusive η'-meson production in the $\Upsilon(1S)$-meson decay. The two dominant

decays are $\Upsilon(1S) \to \gamma^* \to q\bar{q} \to \eta' X$ and $\Upsilon(1S) \to ggg^*(g^* \to \eta' g) \to \eta' X$. The first of these has been estimated from the measured value of the hadronic cross-section $R_{\rm had}$ and the branching ratio $\mathcal{B}(\Upsilon(1S) \to \mu^+\mu^-)$, yielding $\mathcal{B}(\Upsilon(1S) \to \gamma^* \to q\bar{q}) = (8.8 \pm 0.3)\%$ [35], and the CLEO data have been corrected for the $q\bar{q}$ component. In addition, there is also the continuum production from the process $e^+e^- \to \gamma^* \to q\bar{q} \to \eta' X$, which can be estimated from the e^+e^--continuum data below the resonance. These data also provide a good profile of the fragmentation in the process $\gamma^* \to q\bar{q} \to \eta' X$. Typically, the fragmentation processes involving the intermediate $q\bar{q}$ state populate the low-z region, where $z \equiv E_{\eta'}/E_{\rm beam} = 2E_{\eta'}/M$ is the relative η'-meson energy expressed in terms of the $\Upsilon(1S)$-meson mass M. One expects that in the large-z region the process $\Upsilon(1S) \to ggg^*(g^* \to g\eta')$ dominates. Assuming this, we will concentrate here on the intermediate three-gluon (ggg^*) state and analyze the $E_{\eta'}$-spectrum in the large-z region alone. The quality of the fit provides a justification of this procedure a posteriori.

A typical Feynman diagram describing the decay $\Upsilon(1S) \to ggg^*(g^* \to \eta' g) \to \eta' X$ is presented in Fig. 1.

The other 17 diagrams can be obtained from the above one by the permutations of the gluons in the intermediate (virtual) and final states. For the matrix element calculations, we adopted the static limit for the heavy quark–antiquark pair in the orthoquarkonium $\Upsilon(1S)$ system, so that both the quark (b) and antiquark ($\bar{b}$) carry half of the $\Upsilon(1S)$-meson four-momentum, and the velocity-dependent corrections are neglected.

The total decay amplitude can be divided into three parts:

$$\mathcal{M}[\Upsilon(\mathcal{P}) \to \eta'(p_{\eta'}) g(k_1) g(k_2) g(k_3)] = \sum_{i=1}^{3} \mathcal{M}_i, \qquad (9)$$

where each of the three terms $\mathcal{M}_i$ collects the contributions from the diagrams with the virtual gluon of the same four-momentum $p_i = p_{\eta'} + k_i$, with $p_{\eta'}$ and k_i being the four-momenta of the η'-meson and the ith final gluon. The explicit forms of the three contributions $\mathcal{M}_i$ are as follows:

$$\begin{aligned}
\mathcal{M}_1 &= \frac{d_{ABC}}{4\sqrt{N_c}} \frac{g_{\rm s}^3 \sqrt{M}\, \psi(0)\, F_{\eta' g}(p_1^2)}{(\mathcal{P}k_2)(\mathcal{P}k_3)(p_1 p_1')} \qquad (10)\\
&\times \left\{ \frac{4}{M^2} (p_1 \tilde{f}_1^{A*}[f_2^{B*} f_3^{C*} + \tilde{f}_2^{B*} \tilde{f}_3^{C*}] f_V \mathcal{P}) \right.\\
&+ (f_2^{B*} \tilde{f}_3^{C*})(f_1^{A*} f_V) + (f_V \tilde{f}_3^{C*})(f_1^{A*} f_2^{B*})\\
&+ (f_V \tilde{f}_2^{B*})(f_1^{A*} f_3^{C*})\\
&- \frac{2}{p_1^2} \Big[(f_2^{B*} f_3^{C*})(p_1 \tilde{f}_1^{A*} f_V p_1) + (f_V f_3^{C*})(p_1 \tilde{f}_1^{A*} f_2^{B*} p_1)\\
&+ (f_V f_2^{B*})(p_1 \tilde{f}_1^{A*} f_3^{C*} p_1) + (f_2^{B*} \tilde{f}_3^{C*})(p_1 f_1^{A*} f_V p_1)\\
&+ \left. (f_V \tilde{f}_3^{C*})(p_1 f_1^{A*} f_2^{B*} p_1) + (f_V \tilde{f}_2^{B*})(p_1 f_1^{A*} f_3^{C*} p_1) \Big] \right\},\\
\mathcal{M}_2 &= \frac{d_{ABC}}{4\sqrt{N_c}} \frac{g_{\rm s}^3 \sqrt{M}\, \psi(0)\, F_{\eta' g}(p_2^2)}{(\mathcal{P}k_1)(\mathcal{P}k_3)(p_2 p_2')} \qquad (11)\\
&\times \left\{ \frac{4}{M^2} (p_2 \tilde{f}_2^{B*}[f_3^{C*} f_1^{A*} + \tilde{f}_3^{C*} \tilde{f}_1^{A*}] f_V \mathcal{P}) \right.\\
&+ (f_1^{A*} \tilde{f}_3^{C*})(f_2^{B*} f_V) + (f_V \tilde{f}_1^{A*})(f_2^{B*} f_3^{C*})\\
&+ (f_V \tilde{f}_3^{C*})(f_1^{A*} f_2^{B*})\\
&- \frac{2}{p_2^2} \Big[(f_1^{A*} f_3^{C*})(p_2 \tilde{f}_2^{B*} f_V p_2) + (f_V f_1^{A*})(p_2 \tilde{f}_2^{B*} f_3^{C*} p_2)\\
&+ (f_V f_3^{C*})(p_2 \tilde{f}_2^{B*} f_1^{A*} p_2) + (f_1^{A*} \tilde{f}_3^{C*})(p_2 f_2^{B*} f_V p_2)\\
&+ \left. (f_V \tilde{f}_1^{A*})(p_2 f_2^{B*} f_3^{C*} p_2) + (f_V \tilde{f}_3^{C*})(p_2 f_2^{B*} f_1^{A*} p_2) \Big] \right\},\\
\mathcal{M}_3 &= \frac{d_{ABC}}{4\sqrt{N_c}} \frac{g_{\rm s}^3 \sqrt{M}\, \psi(0)\, F_{\eta' g}(p_3^2)}{(\mathcal{P}k_1)(\mathcal{P}k_2)(p_3 p_3')} \qquad (12)\\
&\times \left\{ \frac{4}{M^2} (p_3 \tilde{f}_3^{C*}[f_1^{A*} f_2^{B*} + \tilde{f}_1^{A*} \tilde{f}_2^{B*}] f_V \mathcal{P}) \right.\\
&+ (f_1^{A*} \tilde{f}_2^{B*})(f_3^{C*} f_V) + (f_V \tilde{f}_2^{B*})(f_1^{A*} f_3^{C*})\\
&+ (f_V \tilde{f}_1^{A*})(f_2^{B*} f_3^{C*})\\
&- \frac{2}{p_3^2} \Big[(f_1^{A*} f_2^{B*})(p_3 \tilde{f}_3^{C*} f_V p_3) + (f_V f_2^{B*})(p_3 \tilde{f}_3^{C*} f_1^{A*} p_3)\\
&+ (f_V f_1^{A*})(p_3 \tilde{f}_3^{C*} f_2^{B*} p_3) + (f_1^{A*} \tilde{f}_2^{B*})(p_3 f_3^{C*} f_V p_3)\\
&+ \left. (f_V \tilde{f}_2^{B*})(p_3 f_3^{C*} f_1^{A*} p_3) + (f_V \tilde{f}_1^{A*})(p_3 f_3^{C*} f_2^{B*} p_3) \Big] \right\},
\end{aligned}$$

where d_{ABC} ($A, B, C = 1, \ldots, N_c^2 - 1$ are the colors of the gluons) is the symmetrical constant of the color $SU(N_c)$-group with $N_c = 3$; $g_{\rm s}$ is the strong coupling constant; $(f_V)_{\mu\nu} = \mathcal{P}_\mu \eta_\nu - \mathcal{P}_\nu \eta_\mu$ is the polarization tensor of the $\Upsilon(1S)$-meson, M, $\mathcal{P}_\mu$, η_μ and $\psi(0)$ are the mass of the quarkonium, the four-momentum, the polarization vector, and the non-relativistic wave-function in the position space evaluated at the origin, respectively; $(f_i^A)_{\mu\nu} = k_{i\mu} e_{i\nu}^A - k_{i\nu} e_{i\mu}^A$ and $(\tilde{f}_i^A)_{\mu\nu} = \varepsilon_{\mu\nu\rho\sigma} k_i^\rho e_i^{A\sigma}$ ($i = 1, 2, 3$) are the gluonic field-strength tensor and its dual involving the ith gluon with the polarization vector $e_{i\mu}^A$ and four-momentum $k_{i\mu}$; $p_i = p_{\eta'} + k_i$ is the four-momentum of the virtual gluon, and $p_i' = \mathcal{P} - p_i$. In the above equations the notation is as follows: $(f_1^A f_2^B) = (f_1^A)_{\mu\nu}(f_2^B)^{\nu\mu}$, $(p_1 f_1^A f_2^B p_1) = p_1^\mu (f_1^A)_{\mu\nu} (f_2^B)^{\nu\rho} p_{1\rho}$, etc. It is worth noting that the matrix element satisfies the Bose symmetry under the exchange of gluons, in particular, under the interchange of the first and second gluons $\mathcal{M}_1 \leftrightarrow \mathcal{M}_2$ while the term $\mathcal{M}_3$ remains unchanged.

The function $F_{\eta' g}(p_i^2)$ is the effective vertex function involving the η'-meson and two gluons, one of which is on the mass shell ($k_i^2 = 0$). We shall call this interchangeably also the η'–g transition form factor. A form of this function motivated by the QCD analysis of the $\eta' g^* g$ loop diagram was suggested by Kagan and Petrov [9]:

$$F_{\eta' g}(p^2) \equiv F_{\eta' g^* g}(p^2, 0, m_{\eta'}^2) = \frac{m_{\eta'}^2\, H(p^2)}{p^2 - m_{\eta'}^2}, \qquad (13)$$

where the function $H(p^2)$ was approximated by the constant value $H(p^2) \approx H_0 \simeq 1.7\,{\rm GeV}^{-1}$, extracted from the $J/\psi \to \eta' \gamma$ decay [7]. In a companion paper [36] we argue that the form (13) for the η'–g transition form factor also emerges in the perturbative calculations of this function in the hard-scattering approach by keeping the η'-meson mass. In this approach, the dependence of the function

$H(p^2)$ on the gluon virtuality p^2 is given by the following expression:

$$H(p^2) = \frac{4\pi\alpha_s(Q^2)}{m_{\eta'}^2}\sqrt{3} f_{\eta'} \times \left[1 + A_2(Q^2) - \frac{5}{6} B_2(Q^2)\, G_2^{(g)}(1,\zeta)\right], \quad (14)$$

where $f_{\eta'} \simeq 2f_\pi/\sqrt{3}$ is the η'-meson decay constant expressed in terms of the π-meson decay constant $f_\pi \simeq 133\,\mathrm{MeV}$, $\zeta = m_{\eta'}^2/p^2$, and the function $G_2^{(g)}(1,\zeta)$ has the form [36]

$$G_2^{(g)}(1,\zeta) = \frac{5}{3\zeta} + \frac{2}{\zeta^2} - \frac{4}{\zeta^3} - \frac{1}{\zeta}\left[1 - \frac{1}{\zeta}\right]\left[1 - \frac{4}{\zeta^2}\right]\ln(1-\zeta). \quad (15)$$

In (14) the scale Q^2 in the strong coupling $\alpha_s(Q^2)$, and also in the second Gegenbauer moments $A_2(Q^2)$ and $B_2(Q^2)$ of the quark–antiquark and gluonic LCDAs of the η'-meson, is related with the gluon virtuality p^2, but there is an uncertainty in its precise definition. One of the possibilities is to require that the function $H(p^2)$ is finite at all values of p^2 including the singularity point of the EVF (13), $p^2 = m_{\eta'}^2$, which can be done, for example, by putting $Q^2 = |p^2| + m_{\eta'}^2$.

The dependence of the function $G_2^{(g)}$ on the momentum squared p^2 of the virtual gluon is presented in Fig. 2 with the value $G_2^{(g)}(1,0) = 1/6$ in the large-$|p^2|$ asymptotic region. Since this result is based on the application of perturbation theory, its validity is restricted to the region $|p^2| > p_0^2$, where typically $p_0^2 = 1\,\mathrm{GeV}^2$ (or somewhat higher). In view of this, we shall set $\mathrm{Im}\, G_2^{(g)} = 0$ and ignore the structure in $\mathrm{Re}\, G_2^{(g)}$ in the low-$|p^2|$ region seen in Fig. 2.

As already noted, the functions $A_2(Q^2)$ and $B_2(Q^2)$ in (14) are the second Gegenbauer moments of the quark–antiquark and gluonic light-cone distribution amplitudes (LCDAs) of the η'-meson. The scale μ_0 appearing in the definitions of these moments is set by the initial value in the evolution of the Gegenbauer moments. As the mass of the η'-meson is large, $\sim 1\,\mathrm{GeV}$, it is not a good approximation to neglect it. Assuming further that the evolution of the Gegenbauer moments is valid for the gluons with virtualities larger than $1\,\mathrm{GeV}^2$, we shall take $\mu_0^2 = Q_0^2 \simeq 2\,\mathrm{GeV}^2$.

The total decay width of the $\Upsilon(1S)$-meson into the η'-meson and three gluons, $\Upsilon \to \eta' ggg$, averaged over the quarkonium spin states and summed over the polarizations and colors of the final gluons can be written in the form

$$\begin{aligned}\Gamma_{\eta' X} &\equiv \Gamma[\Upsilon \to \eta' ggg] \\ &= \frac{1}{3!}\,\frac{1}{(2\pi)^8}\,\frac{1}{2M}\int \frac{\mathrm{d}\mathbf{k}_1}{2\omega_1}\,\frac{\mathrm{d}\mathbf{k}_2}{2\omega_2}\,\frac{\mathrm{d}\mathbf{k}_3}{2\omega_3}\,\frac{\mathrm{d}\mathbf{p}_{\eta'}}{2E_{\eta'}} \\ &\times \delta^{(4)}(\mathcal{P} - k_1 - k_2 - k_3 - p_{\eta'}) \\ &\times \frac{1}{3}\sum |\mathcal{M}[\Upsilon \to \eta' ggg]|^2, \end{aligned} \quad (16)$$

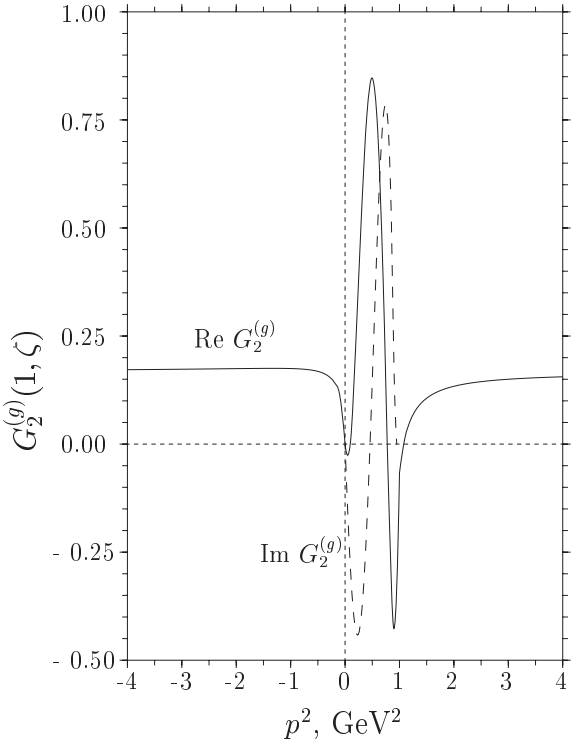

Fig. 2. The real (solid curve) and imaginary (dashed curve) parts of the function $G_2^{(g)}(1,\zeta)$, where $\zeta = m_{\eta'}^2/p^2$, as a function of the momentum squared p^2 of the virtual gluon. We use this function only in the $|p^2| > 1\,\mathrm{GeV}^2$ region

where the factor 1/3! takes into account the identity of the final gluons. The expression for the matrix element squared is rather lengthy and can be found in the appendix, where we have also discussed some technical details of our Monte Carlo integration.

The η'-meson energy distribution function can be defined as follows:

$$\begin{aligned}\frac{\mathrm{d}n}{\mathrm{d}z} &= \frac{1}{\Gamma_{3g}^{(0)}}\,\frac{\mathrm{d}\Gamma_{\eta' X}(z)}{\mathrm{d}z} \\ &= \frac{1}{\Gamma_{3g}^{(0)}}\,\frac{1}{3!}\,\frac{1}{(2\pi)^8}\,\frac{1}{2M}\int \frac{\mathrm{d}\mathbf{k}_1}{2\omega_1}\,\frac{\mathrm{d}\mathbf{k}_2}{2\omega_2}\,\frac{\mathrm{d}\mathbf{k}_3}{2\omega_3}\,\frac{\mathrm{d}\mathbf{p}_{\eta'}}{2E_{\eta'}} \\ &\times \delta^{(4)}(\mathcal{P} - k_1 - k_2 - k_3 - p_{\eta'})\,\delta(z - 2E_{\eta'}/M) \\ &\times \frac{1}{3}\sum |\mathcal{M}[\Upsilon \to \eta' ggg]|^2, \end{aligned} \quad (17)$$

where $\Gamma_{3g}^{(0)}$ is the three-gluon decay width of the $\Upsilon(1S)$-meson in the leading order:

$$\Gamma_{3g}^{(0)} = \frac{16}{9}\left(\pi^2 - 9\right) C_F\, B_F\, \alpha_s^3(M^2)\,\frac{|\psi(0)|^2}{M^2}. \quad (18)$$

Here, $C_F = (N_c^2 - 1)/(2N_c)$ and $B_F = (N_c^2 - 4)/(2N_c)$ are the constants of the color $SU(N_c)$-group, and $\alpha_s(M^2) = g_s^2(M^2)/(4\pi)$ is the strong coupling estimated at the scale of the Υ-meson mass. The α_s corrections to the decay width Γ_{3g} have been known since a long time and are numerically large [37]. However, we do not take them into account, as we have calculated the decay $\Upsilon(1S) \to ggg^*(g^* \to$

$\eta' g$) only in the leading order. One anticipates that in the distribution $\mathrm{d}n/\mathrm{d}z$, a good part of the explicit $O(\alpha_s)$ corrections should drop out, and we are tacitly assuming that the remaining corrections do not greatly influence the energy spectrum derived in the lowest non-trivial order.

3 Numerical analysis of the $\Upsilon(1S) \to \eta' X$ data and the η'-meson LC distribution amplitudes

As the result for the matrix element squared in the decay $\Upsilon(1S) \to ggg^*(g^* \to \eta' g)$ is not yet available in the literature, we shall give its explicit expression in this paper. In that context we note that it is sufficient to have the expressions for one of the diagonal terms $|\mathcal{M}_i|^2$ $(i = 1, 2, 3)$ and one of the non-diagonal terms $\mathcal{M}_i \mathcal{M}_j^*$ $(i \neq j)$, as the others can be obtained by using Bose symmetry. With this, the expressions for the components $(1/3)\sum |\mathcal{M}_1|^2$, derived from (10), and $(1/3)\sum \mathcal{M}_1 \mathcal{M}_2^* + \text{c.c.}$, resulting from the cross terms in (10) and (11) in $|\mathcal{M}|^2$, are given in the appendix.

We start our numerical calculations by reproducing the already known results for the η'-meson energy spectrum $\mathrm{d}n/\mathrm{d}z$ [35,22], as this provides a good consistency check of our calculations. For this purpose, the spectrum in Fig. 3 is calculated with the same set of phenomenological parameters as has been used in [22] for the following three input forms[1].

(a) A slowly falling EVF:

$$F_{\eta' g}(p^2) \simeq 2.1\,\mathrm{GeV}^{-1}\,[\alpha_s(p^2)/\alpha_s(m_{\eta'}^2)]\,,$$

where the two-loop expression is used for the strong coupling α_s.

(b) A rapidly falling EVF of the form (13) with the function $H(p^2)$ approximated by the constant value $H(p^2) \simeq 1.7\,\mathrm{GeV}^{-1}$.

(c) An intermediate EVF: $F_{\eta' g}(p^2) \simeq 12.5\,\mathrm{GeV}/(p^2 + M_0^2)$ with $M_0 = 2.25\,\mathrm{GeV}$.

The shapes of the η'-meson energy spectrum resulting from these EVFs are presented in Fig. 3.

The experimental points in the decay $\Upsilon(1S) \to \eta' X$ shown in this figure are taken from [35]. Our results are in agreement with the ones in [22], and we confirm the previous observation that curve (b), corresponding to the rapidly falling EVF, is in reasonable agreement with the experimental data in the hard-energy region $z \geq 0.7$ [35]. Note that the allowed kinematic domain of the variable z is $z_0 < z < 1 + z_0^2/4$, where $z_0 = 2m_{\eta'}/M$. The region $1 < z < 1 + z_0^2/4$ is too small to be resolved experimentally, given the statistics of the CLEO data [35], and hence the energy distribution above $z = 1$ is included in the last energy bin $0.9 < z < 1.0$.

[1] We thank Alex Kagan for providing us the input parameters used in their analysis of Fig. 3. It should be noted that in the rest of our paper we have used the input parameters displayed in Table 1

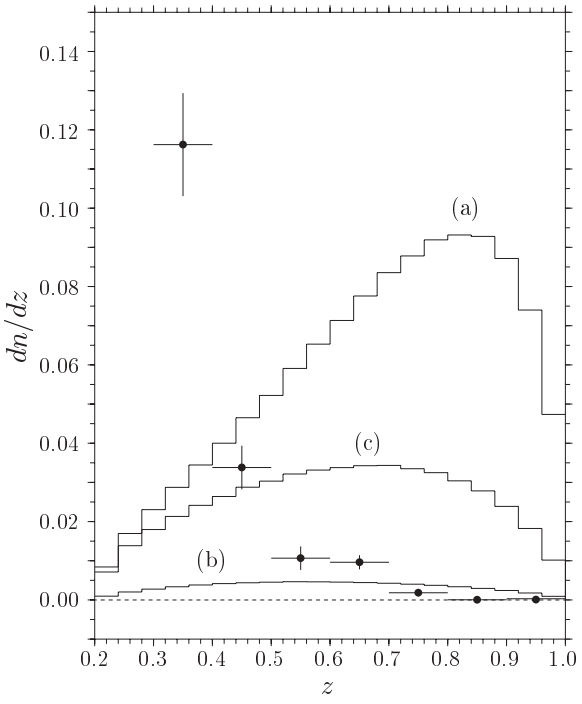

Fig. 3. The energy spectrum of the η'-meson in the decay $\Upsilon(1S) \to \eta' ggg \to \eta' X$ for the three assumed phenomenological models for the $\eta' g^* g$ vertex given in the text, in comparison with the data from the CLEO collaboration [35]. Note that only the data points for $z = 2E_{\eta'}/M \geq 0.7$ are relevant for comparison with the theoretical models

Table 1. Input parameters used in the numerical analysis

M	$= 9.46\,\mathrm{GeV}$	m_c	$= 1.3\,\mathrm{GeV}$
$m_{\eta'}$	$= 958\,\mathrm{MeV}$	m_b	$= 4.3\,\mathrm{GeV}$
f_π	$= 133\,\mathrm{MeV}$	$\Lambda^{(4)}_{\mathrm{QCD}}$	$= 305\,\mathrm{MeV}$
μ_0^2	$= 2\,\mathrm{GeV}^2$		

Let us now turn to the analysis of the perturbative-QCD based form of the effective vertex presented in (13)–(15). To fit the parameters $B_2^{(q)}(\mu_0^2)$ and $B_2^{(g)}(\mu_0^2)$ from the existing experimental data on the $\Upsilon(1S) \to \eta' ggg \to \eta' X$ decay, it is convenient to derive first an approximate numerical formula for the η'-meson energy spectrum. This expression will come in handy for subsequent comparison with other independent calculations and will also facilitate undertaking an analysis of the data in future by the experimental groups themselves.

As the amplitude of the process considered is linear in $B_2^{(q)}$ and $B_2^{(g)}$, the energy spectrum $\mathrm{d}n/\mathrm{d}z$ is quadratic in these parameters. The general form for the energy spectrum in the decay $\Upsilon(1S) \to \eta' ggg \to \eta' X$ can be written as follows (suppressing in this equation the scale-dependence of the coefficients for ease of writing):

$$\frac{\mathrm{d}\tilde{n}}{\mathrm{d}z}(z, B_2^{(q)}, B_2^{(g)}) = C_{00}(z) + C_{0q}(z) B_2^{(q)} + C_{0g}(z) B_2^{(g)} + C_{qq}(z)[B_2^{(q)}]^2 + C_{qg}(z) B_2^{(q)} B_2^{(g)} + C_{gg}(z)[B_2^{(g)}]^2. \quad (19)$$

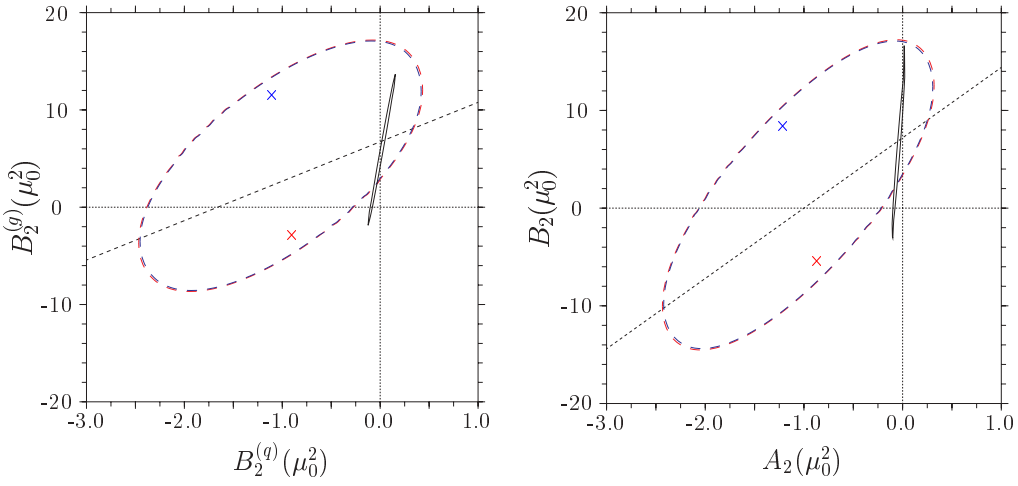

Fig. 4. The $\pm 1\sigma$ contours (long-dashed curves) in the $B_2^{(g)}(\mu_0^2)$–$B_2^{(q)}(\mu_0^2)$ parameter space (left frame) and for the $B_2(\mu_0^2)$–$A_2(\mu_0^2)$ Gegenbauer moments (right frame) resulting from the analysis of the last three experimental bins in the η'-meson energy spectrum in the process $\Upsilon(1S) \to \eta' X$ measured by the CLEO collaboration [35]. The crosses ($\times$) represent the two solutions with the minimum χ^2 given in the text. The narrow solid contours result from the analysis of the data on the η'–γ transition form factor, scaled from [25]. The short-dashed lines in both the frames result by demanding that the vertex function $F_{\eta' g}(p^2)$ remains positive for all values of $p^2 > m_{\eta'}^2$, admitting only the regions below these lines. Note that all the contours correspond to using $\mu_0^2 = 2\,\mathrm{GeV}^2$

Table 2. The coefficients in the interpolating function $\mathrm{d}\tilde{n}/\mathrm{d}z$ defined in the text for the decay $\Upsilon(1S) \to \eta' X$. The numbers in brackets are from the Monte Carlo statistical errors

z	$C_{00}(z)$	$C_{0q}(z)$	$C_{0g}(z)$	$C_{qq}(z)$	$C_{qg}(z)$	$C_{gg}(z)$
$0.6 \div 0.7$	1.9172(27)	2.5187(36)	−0.3108(13)	0.8744(19)	−0.1888(07)	0.0146(06)
$0.7 \div 0.8$	1.6750(25)	2.2368(34)	−0.2583(12)	0.7953(18)	−0.1560(07)	0.0122(06)
$0.8 \div 0.9$	1.2768(21)	1.7344(29)	−0.1855(10)	0.6343(15)	−0.1097(06)	0.0089(05)
$0.9 \div 1.0$	0.6475(17)	0.8945(17)	−0.0866(07)	0.3396(09)	−0.0484(05)	0.0044(05)

We have generated the theoretical $E_{\eta'}$-spectrum, using a high statistics Monte Carlo phase space programme, with fixed values of the coefficients $B_2^{(q)}(\mu_0^2)$ and $B_2^{(g)}(\mu_0^2)$, and have varied their values over a certain range to numerically determine the dependence of the spectrum on these coefficients. Other parameters in our numerical analysis are listed in Table 1, which are the same as the ones used in the analysis of the η'–γ and η–γ transition form factors [25], for the sake of consistency, as we are going to make use of this analysis. We have not included any errors on m_c, m_b and $\Lambda^{(4)}_{\mathrm{QCD}}$, as the parametric uncertainties from the Gegenbauer coefficients which we study are by far the largest. The coefficients $C_{ab}(z)$ $[a, b = 0, q, g]$ for the four bins of the η'-meson energy spectrum are presented in Table 2. The numbers presented in parentheses represent the statistical error of our Monte Carlo calculations, for which we have used the Monte Carlo phase space generator FOWL from the CERN Library of programmes. With the help of the program MINUIT [38], the following best-fit values of the parameters $B_2^{(q)}(\mu_0^2)$ and $B_2^{(g)}(\mu_0^2)$ are obtained:

$$\begin{aligned} B_2^{(q)}(\mu_0^2) &= -0.89^{+1.32}_{-1.58}, \quad B_2^{(g)}(\mu_0^2) = -2.86^{+20.04}_{-5.80}, \\ \chi^2 &= 2.45, \\ B_2^{(q)}(\mu_0^2) &= -1.09^{+1.51}_{-1.36}, \quad B_2^{(g)}(\mu_0^2) = 11.53^{+5.55}_{-20.09}, \\ \chi^2 &= 2.37, \end{aligned} \tag{20}$$

for the last three experimental bins with $z > 0.7$ (the stated χ^2 corresponds to three degrees of freedom), and

$$\begin{aligned} B_2^{(q)}(\mu_0^2) &= -0.77^{+0.73}_{-0.78}, \quad B_2^{(g)}(\mu_0^2) = -4.36^{+6.28}_{-4.46}, \\ \chi^2 &= 24.13, \\ B_2^{(q)}(\mu_0^2) &= -1.29^{+0.76}_{-0.73}, \quad B_2^{(g)}(\mu_0^2) = 12.51^{+4.53}_{-6.33}, \\ \chi^2 &= 23.69, \end{aligned} \tag{21}$$

for the four experimental data points in the large-z region ($z > 0.6$). The minimum χ^2 of the fit in the last case, namely $\chi^2 \simeq 24$ for four degrees of freedom, is unacceptably large. Thus, as already observed in [35], only the last three bins in the energy spectrum are dominated by the $\Upsilon(1S) \to \eta' ggg \to \eta' X$ decay. Following this, we concentrate on the analysis of the last three bins with $z \geq 0.7$. The 1σ contours both in the Gegenbauer coefficients $(B_2^{(q)}(\mu_0^2),\ B_2^{(g)}(\mu_0^2))$ and in the Gegenbauer moments $(A_2(\mu_0^2),\ B_2(\mu_0^2))$ are presented as long-dashed curves in Fig. 4.

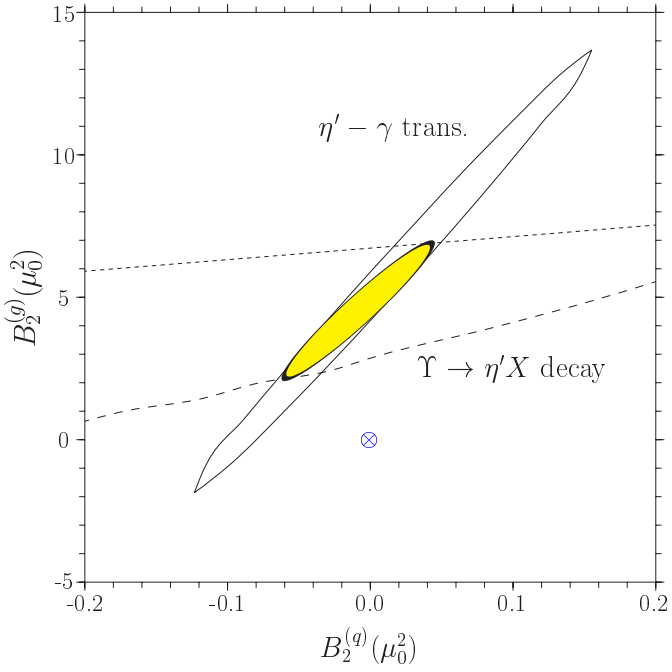

Fig. 5. The combined fit for the parameters $B_2^{(q)}(\mu_0^2 = 2\,\mathrm{GeV}^2)$ and $B_2^{(g)}(\mu_0^2 = 2\,\mathrm{GeV}^2)$ from the data on the η'–γ transition form factor (solid curve) and $\Upsilon(1S) \to \eta' X$ decay (long-dashed and short-dashed curves) with the requirement that the vertex $F_{\eta' g}(p^2)$ remains positive definite in the entire p^2 region. The resulting 1σ contour (combined best fit) is shown by the yellow (shaded) region. The point denoted by $\otimes$ corresponds to the asymptotic light-cone distribution amplitude

The best-fit values (20) are denoted by the crosses ($\times$). The narrow contours (solid curves) also shown in these figures result from the analysis of the data on the η'–γ transition form factor [25]. As we are using $\mu_0^2 = 2\,\mathrm{GeV}^2$ in our analysis, the results from [25] have been rescaled from $\mu_0^2 = 1\,\mathrm{GeV}^2$ to $\mu_0^2 = 2\,\mathrm{GeV}^2$ with the help of (3) and (4) for $n = 2$. We note that the analysis of the η'–γ data, being more sensitive to the quark–antiquark LCDA of the η'-meson, provides a much more precise determination of the parameter $B_2^{(q)}(\mu_0^2)$ and hence of the Gegenbauer moment $A_2(\mu_0^2)$, than the one that can be determined at present from the CLEO data on $\Upsilon(1S) \to \eta' X$. However, what concerns the coefficient $B_2^{(g)}(\mu_0^2)$, and also the Gegenbauer moment $B_2(\mu_0^2)$, the CLEO data on $\Upsilon(1S) \to \eta' X$, despite its statistical limitations, has cut out some of the allowed parameter region from the η'–γ analysis. The additional constraint that follows from demanding that the vertex function $F_{\eta' g}(p^2)$ remains positive definite for all values of $p^2 > m_{\eta'}^2$ is shown through the short-dashed lines in these figures, admitting only the parameter space below these lines. We will discuss this constraint in more detail below.

A blow up of the overlapping region in the parameter space $(B_2^{(g)}(\mu_0^2), B_2^{(q)}(\mu_0^2))$ is shown in Fig. 5.

Here, the 1σ contours following from the η'–γ transition form factor analysis and the $\Upsilon(1S) \to \eta' X$ decay fit are shown through the solid and dashed curves, respectively. In drawing the allowed parameter space from the $\Upsilon(1S) \to \eta' X$ decay fit, we have imposed the additional condition that the $\eta' g^* g$ vertex function $F_{\eta' g}(p^2)$ for $p^2 > m_{\eta'}^2$ has the same sign as the corresponding function calculated with the asymptotic forms of the η'-meson quark–antiquark and gluonic LCDAs which is defined as positive definite in the entire p^2 region. With (13) taken into account, this condition implies $H(p^2) > 0$ and results [with the help of the explicit form (14) of the function $H(p^2)$] in the following inequalities:

$$B_2(\mu_0^2) \le \frac{36}{5}\left[1 + A_2(\mu_0^2)\right], \tag{22}$$

$$B_2^{(g)}(\mu_0^2) \le \frac{36 + (36 - 5\rho_2^{(q)})\, B_2^{(q)}(\mu_0^2)}{5 - 36\rho_2^{(g)}},$$

where the function $G_2^{(g)}(1, \zeta)$ (15) is approximated by its value 1/6 in the large-$|p^2|$ asymptotics. The values $\rho_2^{(q)} = 2.86$ and $\rho_2^{(g)} = -0.01$ were taken for the constrained parameters in the numerical analysis. The positivity constraint removes the larger values of $B_2^{(g)}(\mu_0^2)$ above the short-dashed curve in Fig. 5, which would otherwise force the vertex function to cross the zero at some value of p^2 and become negative. This is exemplified below for specific values of the Gegenbauer coefficients. The resulting combined best fit of the parameters $B_2^{(q)}(\mu_0^2)$ and $B_2^{(g)}(\mu_0^2)$ is shown as the colored (shaded) region. This yields the following correlated values:

$$B_2^{(q)}(\mu_0^2) = -0.008 \pm 0.054, \qquad B_2^{(g)}(\mu_0^2) = 4.6 \pm 2.5,$$
$$A_2(\mu_0^2) = -0.054 \pm 0.029, \qquad B_2(\mu_0^2) = 4.6 \pm 2.7, \tag{23}$$

with the central values having $\chi^2 = 2.66$ for three degrees of freedom. For comparison, the point shown as $\otimes$, corresponding to the asymptotic LCDA, has $\chi^2 = 8.41$ for three degrees of freedom. Thus, the asymptotic form of the η'-meson LCDA is not favored by our analysis.

The shapes of the quark–antiquark and gluonic LCDAs are presented in Fig. 6 (left frame); the resulting η'–g transition form factor $F_{\eta' g}(p^2)$ corresponding to these LCDAs is also shown in this figure (right frame). The solid and dotted curves in this figure correspond to the asymptotic LCDA and the combined best-fit values of the Gegenbauer coefficients (23), respectively. We also show, for the sake of illustration, representative LCDAs with the Gegenbauer coefficients having the values $B_2^{(q)}(2\,\mathrm{GeV}^2) = 0.15$ and $B_2^{(g)}(2\,\mathrm{GeV}^2) = 13.5$. These parametric values are taken from the analysis in [25], but are in conflict with the positive definiteness of the vertex function $F_{\eta' g}(p^2)$, as shown by the dashed curve for $F_{\eta' g}(p^2)$. In fact, the constraint of positivity on the effective vertex function cuts out regions in the parameter space $B_2^{(q)}(2\,\mathrm{GeV}^2) > 0.045$ and $B_2^{(g)}(2\,\mathrm{GeV}^2) > 7.1$, as otherwise the contribution from the gluonic LCDA starts to dominate, which makes the vertex function $F_{\eta' g}(p^2)$ negative for some range of p^2 considered here and in [25]. Thus, the positivity criterion

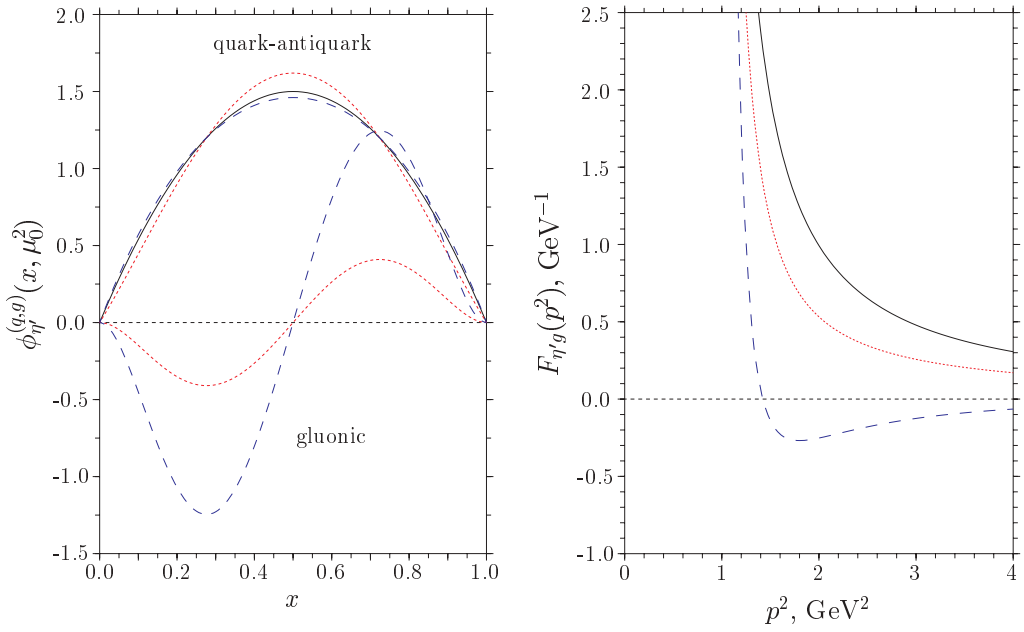

Fig. 6. The η'-meson quark–antiquark and gluonic LCDAs $\phi_{\eta'}^{(q,g)}(x,\mu_0^2)$ as a function of x (left frame), and the resulting η'–g transition form factor $F_{\eta' g}(p^2)$ (right frame). The solid curves correspond to the asymptotic quark–antiquark LCDA, while the LCDAs for the combined best-fit values of the Gegenbauer coefficients given in (23) are drawn as dotted curves. The LCDAs with the values $B_2^{(q)} = 0.15$ and $B_2^{(g)} = 13.5$, which are allowed within 1σ from the analysis of the data on the η'–γ transition form factor [25], are presented as dashed curves. Note that for this case the function $F_{\eta' g}(p^2)$ is no longer positive definite, as shown in the right frame

provides an effective constraint on the magnitude of the coefficient $B_2^{(g)}(\mu_0^2)$, significantly reducing the otherwise allowed range in (7). In the context of our analysis, we note that the asymptotic η'-meson LCDA provides a fair description (though not the best fit) of the current data on $\Upsilon(1S) \to ggg^*(g^* \to \eta' g) \to \eta' X$, and hence one anticipates that the subasymptotic corrections in the LCDAs, and the vertex function $F_{\eta' g}(p^2)$, while important in the analysis of data, are not dominant[2].

The EVF $F_{\eta' g}(p^2)$ and the function $m_{\eta'}^2 H(p^2)$ for the combined best-fit values (23) are presented in Fig. 7.

The η'-meson energy spectrum for the EVF motivated by the perturbative-QCD analysis is presented in Fig. 8 in comparison with the experimental data [35] and the spectrum corresponding to the "rapidly falling" form of the EVF [22] labeled by the constant value of the function $H(p^2) = H_0 \simeq 1.7\,\text{GeV}^{-1}$. The second dotted line labeled by $H_{\rm as}(p^2)$ corresponds to the EVF when only the asymptotic form of the η'-meson LCDA ($B_2^{(q)} = 0$ and $B_2^{(g)} = 0$) is taken into account. The yellow (shaded) region demarcates the spectrum with the Gegenbauer coefficients having values in the range of the combined best fit (23). The blue (solid) curve lying inside this region corresponds to the best-fit values (20) obtained from the analysis of the $\Upsilon(1S) \to \eta' X$ decay only. From Fig. 8 it is seen that the rapidly falling phenomenological EVF with $H_0 = 1.7\,\text{GeV}^{-1}$ gives a harder η'-meson energy spectrum for the large-z region compared to the CLEO data. The spectrum with the asymptotic form of the η'-meson LCDA is well correlated with the experimental point in the bin $0.7 \le z \le 0.8$, but overestimates the data in the other two bins. It should be noted that the last two bins (especially the bin $0.8 \le z \le 0.9$) are very uncertain in the current data, which have to be statistically improved to draw sharper conclusions.

[2] The approximate validity of the asymptotic transition form factors involving the π-, η- and η'-mesons compared to the data, observed in [39,40], also suggests that the coefficient $B_2^{(g)}(\mu_0^2)$ in the η'-meson is bounded by these data. The gluonic components of the π- and the η-meson LCDAs are small in any case

4 Summary

We have calculated the η'-meson energy spectrum in the decay $\Upsilon(1S) \to \eta' ggg \to \eta' X$ in leading-order perturbative QCD in the static quark limit for orthoquarkonium. Assuming some phenomenological vertex functions, our results are in agreement with the ones obtained earlier in [22]. In our analysis, the η'-meson is described in the leading-twist (twist-two) accuracy in terms of the quark–antiquark and gluonic LCDAs for which the asymptotic and the first non-asymptotic terms are taken into account. In this approximation, the $\eta' g^* g$ EVF depends essentially on the Gegenbauer coefficients $B_2^{(q)}(\mu_0^2)$ and $B_2^{(g)}(\mu_0^2)$. They are determined from the CLEO data on $\Upsilon(1S) \to \eta' X$ in the large-z region ($z \ge 0.7$) of the η'-meson energy spectrum [35], which is well explained by

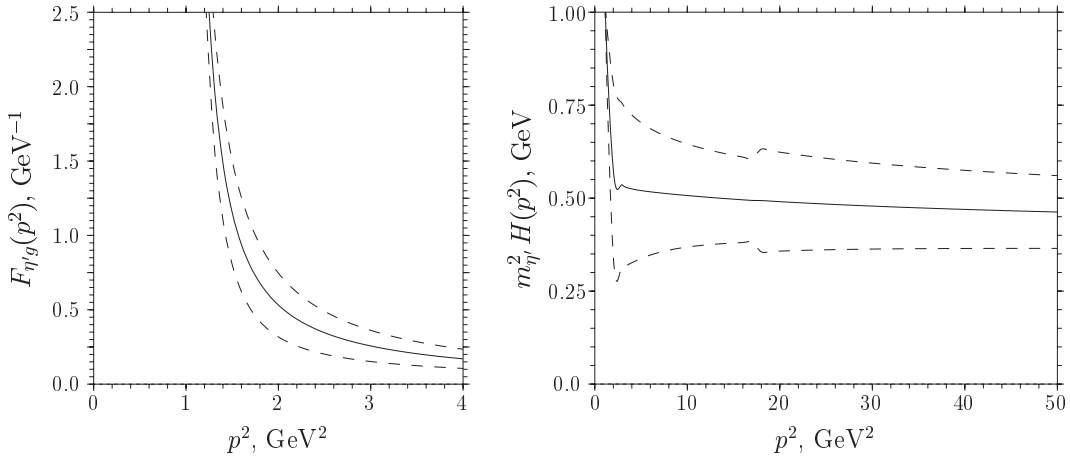

Fig. 7. The η'–g transition form factor $F_{\eta' g}(p^2)$, defined in (13) (left frame), and the function $m_{\eta'}^2 H(p^2)$, defined in (14) (right frame), as functions of the gluon virtuality p^2. The various curves correspond to the input values of the Gegenbauer coefficients $B_2^{(q)}(\mu_0^2)$ and $B_2^{(g)}(\mu_0^2)$ resulting from the combined best fit shown in Fig. 5. The solid curves correspond to the central values of the fit, while the dashed curves are drawn for the parameters corresponding to the uppermost and lowermost allowed values of the combined best-fit contour shown in Fig. 5

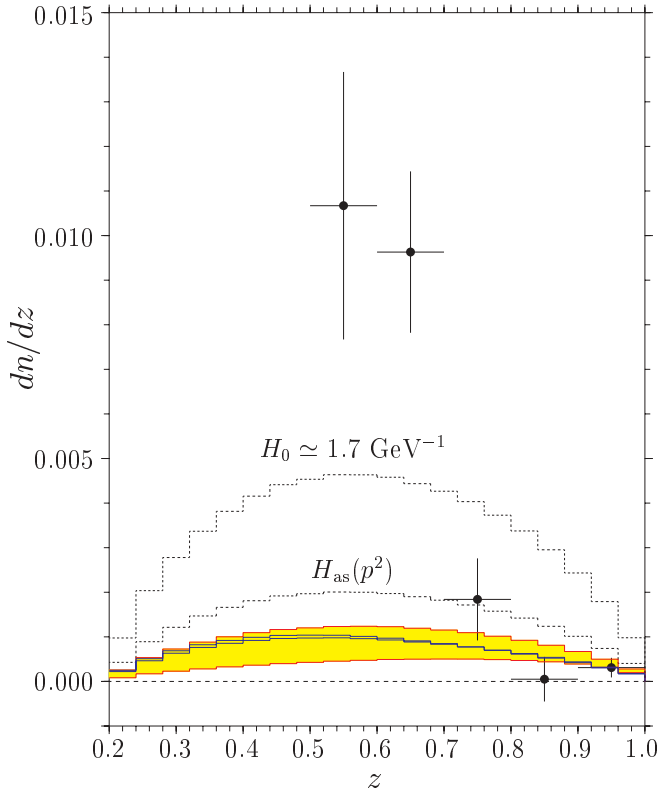

Fig. 8. Energy spectrum of the η'-meson in the decay $\Upsilon(1S) \to \eta' X$. The upper dotted curve corresponds to a constant value of the function $H(p^2) = H_0 \simeq 1.7\,\text{GeV}^{-1}$, and the curve marked as $H_{\rm as}(p^2)$ corresponds to the asymptotic form of the η'-meson LCDA (i.e., $B_2^{(q)} = 0$ and $B_2^{(g)} = 0$). The spectrum with the Gegenbauer coefficients in the combined best-fit range of these parameters is shown by the yellow (shaded) region. The blue (solid) curve inside this region corresponds to the best-fit values of the Gegenbauer coefficients from the analysis of the $\Upsilon(1S) \to \eta' X$ data alone

our perturbative-QCD approach. However, the resulting 1σ contour in the Gegenbauer coefficients has a large dispersion. Combining the analysis of the $\Upsilon(1S) \to \eta' X$ data with an earlier analysis of the (η', η)–γ transition form factors in a similar theoretical framework [25], and requiring additionally that the vertex function $F_{\eta' g}(p^2)$ remains positive definite in the entire $p^2 > m_{\eta'}^2$ region, yield a much improved determination of the Gegenbauer coefficients, yielding $B_2^{(q)}(2\,\text{GeV}^2) = -0.008 \pm 0.054$ and $B_2^{(g)}(2\,\text{GeV}^2) = 4.6 \pm 2.5$. Our analysis improves the phenomenological profile of the LCDAs in the η'-meson, and in turn yields a better determination of the vertex function $F_{\eta' g}(p^2)$ compared to the earlier estimates of the same. The resulting function (the η'–gluon transition form factor) is presented in this paper including the η'-meson mass effects.

Acknowledgements. We would like to thank Alex Kagan, Christoph Greub, Peter Minkowski and Sheldon Stone for numerous helpful discussions. We also thank Gustav Kramer for his comments on the earlier version of this manuscript. The work of A.Ya.P. has been supported by the Schweizerischer Nationalfonds.

A Matrix element squared for the decay $\Upsilon(1S) \to ggg^*(g^* \to \eta' g)$

In Sect. 2, we have displayed explicitly the terms $\mathcal{M}_i$ ($i = 1, 2, 3$) in the decomposition of the total amplitude of the decay $\Upsilon(1S) \to \eta' ggg$ in the leading-order perturbative QCD [(10)–(12)]. Squaring this amplitude results in very lengthy expressions. Nevertheless, it is possible to present compact analytical expressions for some parts of the matrix element squared. In particular, the square of the term $\mathcal{M}_1$, summed over the polarizations and colors of the fi-

nal gluons and averaged over the polarization states of the Υ-meson, can be written as follows:

$$\frac{1}{3}\sum|\mathcal{M}_1|^2 = \frac{512}{3}\,C_F B_F \pi^3 \alpha_s^3(M^2) \times \frac{|\psi(0)|^2}{M}\left|F_{\eta' g}(p_1^2)\right|^2 \frac{J_{11}(\mathcal{P},k_i,p_i)}{(\mathcal{P}k_2)^2(\mathcal{P}k_3)^2(p_1' p_1)^2(p_1^2)^2}, \tag{24}$$

where the well-known property of the symmetrical constants d_{ABC} of the color $SU(N_c)$-group has been used:

$$\sum_{C,D=1}^{N_c^2-1} d_{ACD}\,d_{BCD} = \frac{N_c^2-4}{N_c}\,\delta_{AB} \equiv 2B_F\,\delta_{AB}, \tag{25}$$

and the dynamical function $J_{11}(\mathcal{P},k_i,p_i)$ has the form

$$\begin{aligned}
&J_{11}(\mathcal{P},k_i,p_i)\\
&= 4M^2(k_1p_1)^2\\
&\times\left[(k_2k_3)^2(\mathcal{P}p_1)^2+(k_2p_1)^2(\mathcal{P}k_3)^2+(k_3p_1)^2(\mathcal{P}k_2)^2\right]\\
&+4M^2(p_1^2)^2(k_2k_3)^2\left[(k_1k_2)^2+(k_1k_3)^2\right]\\
&+8M^2p_1^2(p_1k_1)^2(k_2k_3)\left[(k_2k_3)^2-(k_2p_1)(k_3p_1)\right]\\
&-8M^2p_1^2(p_1k_1)(k_2k_3)^2\left[(k_1k_2)(k_2p_1)+(k_1k_3)(k_3p_1)\right]\\
&+2M^2p_1^2(M^2-p_1^2)\\
&\times\left\{\left[(k_1k_2)(k_3p_1)-(k_1k_3)(k_2p_1)\right]^2-(p_1k_1)^2(k_2k_3)^2\right\}\\
&+2p_1^2(M^2-p_1^2)\left[M^2(k_2k_3)+2(\mathcal{P}k_2)(\mathcal{P}k_3)\right]\\
&\times\Big[p_1^2(k_1k_2)(k_1k_3)-(k_1p_1)(k_1k_2)(k_3p_1)\\
&\quad-(k_1p_1)(k_1k_3)(k_2p_1)\Big].
\end{aligned} \tag{26}$$

It is easy to check that this function is invariant under the interchange $(k_2,p_2) \leftrightarrow (k_3,p_3)$, which reflects the Bose symmetry for the set of the Feynman diagrams considered. The other two dynamical functions $J_{22}(\mathcal{P},k_i,p_i)$ and $J_{33}(\mathcal{P},k_i,p_i)$ originating from the squares of the terms $\mathcal{M}_2$ and $\mathcal{M}_3$, respectively, can be obtained from $J_{11}(\mathcal{P},k_i,p_i)$ by the obvious replacements $(k_1,p_1) \leftrightarrow (k_2,p_2)$ and $(k_1,p_1) \leftrightarrow (k_3,p_3)$.

The differential width of the $1 \to 4$ decay has a non-trivial dependence on five variables (three angles can be integrated out trivially) in the rest frame of the decaying particle. In the Monte Carlo generator, the matrix element squared is rewritten in terms of the following dimensionless variables:

$$x_i = \frac{2(\mathcal{P}k_i)}{M^2}, \qquad y_i = \frac{p_i^2}{M^2}, \qquad i = 1,2,3, \tag{27}$$

which satisfy the relation

$$x_1+x_2+x_3+y_1+y_2+y_3 = 2+z_0^2/4, \tag{28}$$

where $z_0 = 2m_{\eta'}/M$ is the relative mass of the η'-meson.

The experimentally measured quantity is the η'-meson energy spectrum – the number of $\Upsilon \to \eta' X$ events Δn_i inside the energy bin with the central value z_i and the width Δz. This can be calculated theoretically in the Monte Carlo approach which we have used. In particular, as an input for the calculation of the contribution coming from $|\mathcal{M}_1|^2$, the following equation was used:

$$\begin{aligned}
\frac{\Delta n_i^{(11)}}{\Delta z} &= \int\limits_{z_i-\Delta z/2}^{z_i+\Delta z/2} \mathrm{d}z\,\delta(z-2E_{\eta'}/M)\int\frac{\mathrm{d}\mathbf{k}_1}{2\omega_1}\frac{\mathrm{d}\mathbf{k}_2}{2\omega_2}\frac{\mathrm{d}\mathbf{k}_3}{2\omega_3}\frac{\mathrm{d}\mathbf{p}_{\eta'}}{2E_{\eta'}}\\
&\times\delta^{(4)}(\mathcal{P}-k_1-k_2-k_3-p_{\eta'})\\
&\times\frac{|MF_{\eta' g}(y_1)|^2}{64\pi^5(\pi^2-9)M^4}\,\frac{\mathcal{F}_{11}(x_i,y_i,z_0)}{[y_1x_2x_3(2-2y_1-x_2-x_3)]^2},
\end{aligned} \tag{29}$$

where the representation (24) for $|\mathcal{M}_1|^2$ was put into the definition of $\mathrm{d}n/\mathrm{d}z$ (17). The dimensionless function $\mathcal{F}_{11}(x_i,y_i,z_0)$ is related to the function $J_{11}(\mathcal{P},k_i,p_i)$ as follows:

$$J_{11}(\mathcal{P},k_i,p_i) = \frac{M^{14}}{128}\,\mathcal{F}_{11}(x_i,y_i,z_0). \tag{30}$$

The first integral in (29) serves for a selection of the generated Monte Carlo events with the η'-meson energy being inside the bin $z_i - \Delta z/2 < z < z_i + \Delta z/2$.

In the same way all the other contributions from the matrix element squared were implemented in the numerical analysis. In particular, the contribution to the energy spectrum coming from the product $(1/3)\sum\mathcal{M}_1^*\mathcal{M}_2 + \text{c.c.}$ can be written as

$$\begin{aligned}
\frac{\Delta n_i^{(12)}}{\Delta z} &= \int\limits_{z_i-\Delta z/2}^{z_i+\Delta z/2} \mathrm{d}z\,\delta(z-2E_{\eta'}/M)\int\frac{\mathrm{d}\mathbf{k}_1}{2\omega_1}\frac{\mathrm{d}\mathbf{k}_2}{2\omega_2}\frac{\mathrm{d}\mathbf{k}_3}{2\omega_3}\frac{\mathrm{d}\mathbf{p}_{\eta'}}{2E_{\eta'}}\\
&\times\delta^{(4)}(\mathcal{P}-k_1-k_2-k_3-p_{\eta'})\\
&\times\frac{M^2F_{\eta' g}(y_1)F_{\eta' g}(y_2)}{64\pi^5(\pi^2-9)M^4}\\
&\times\frac{2\mathcal{F}_{12}(x_i,y_i,z_0)}{y_1y_2x_1x_2x_3^2(2-2y_1-x_2-x_3)(2-2y_2-x_1-x_3)}.
\end{aligned} \tag{31}$$

However, we have not been able to find compact expressions for the non-diagonal terms $(1/3)\sum\mathcal{M}_i\mathcal{M}_j^*$ $(i \neq j)$. We present here instead the dimensionless function $\mathcal{F}_{12}(x_i,y_i,z_0)$ in the form of a series in powers of $z_0^2/4 = m_{\eta'}^2/M^2$:

$$\mathcal{F}_{12}(x_i,y_i,z_0) = \sum_{k=0}^{5} f_{12}^k(x_i,y_i)\left(\frac{z_0^2}{4}\right)^k, \tag{32}$$

where the functions $f_{12}^k(x_i,y_i)$ are as follows:

$$\begin{aligned}
f_{12}^0 = \frac{1}{4}\Big\{&(\Delta x_{12})^4(\Delta y_{12})^2-4(\Delta x_{12})^3(\Delta y_{12})^3\\
&+4(\Delta x_{12})^3\Delta y_{12}y_3^2\\
&+8(\Delta x_{12})^3\Delta y_{12}y_3(x_{12}+x_3-2)\\
&+4(\Delta x_{12})^3\Delta y_{12}(x_{12}^2+2x_{12}x_3-4x_{12}+x_3^2-4x_3+4)\\
&+5(\Delta x_{12})^2(\Delta y_{12})^4\\
&+2(\Delta x_{12})^2(\Delta y_{12})^2y_3(-2x_{12}-4x_3+7)
\end{aligned} \tag{33}$$

$$
\begin{aligned}
&+ 2(\Delta x_{12})^2(\Delta y_{12})^2 \\
&\times (-x_{12}^2 - 6x_{12}x_3 + 7x_{12} - 2x_3^2 + 9x_3 - 8) \\
&- 2\Delta x_{12}(\Delta y_{12})^5 \\
&+ 4\Delta x_{12}(\Delta y_{12})^3 y_3^2(-x_3 - 2) \\
&+ 4\Delta x_{12}(\Delta y_{12})^3 y_3(-x_{12}x_3 - 2x_{12} + 2x_3) \\
&+ 4\Delta x_{12}(\Delta y_{12})^3 x_{12}(-x_{12} + x_3 + 1) \\
&+ 2\Delta x_{12}\Delta y_{12} y_3^4(2x_3 + 5) \\
&+ 4\Delta x_{12}\Delta y_{12} y_3^3(3x_{12}x_3 + 2x_{12} + 2x_3^2 - 12x_3 + 12) \\
&+ 4\Delta x_{12}\Delta y_{12} y_3^2 \\
&\times \Big(3x_{12}^2x_3 + 4x_{12}x_3^2 - 17x_{12}x_3 + 19x_{12} + x_3^3 - 11x_3^2 \\
&\quad +36x_3 - 36\Big) \\
&+ 4\Delta x_{12}\Delta y_{12} y_3 \\
&\times \Big(x_{12}^3x_3 + 2x_{12}^2x_3^2 - 12x_{12}^2x_3 + 14x_{12}^2 + x_{12}x_3^3 \\
&\quad -16x_{12}x_3^2 + 54x_{12}x_3 - 52x_{12} - 4x_3^3 \\
&\quad +28x_3^2 - 64x_3 + 48\Big) \\
&+ 2\Delta x_{12}\Delta y_{12} \\
&\times \Big(-x_{12}^4 - 6x_{12}^3x_3 + 14x_{12}^3 - 8x_{12}^2x_3^2 + 44x_{12}^2x_3 \\
&\quad -56x_{12}^2 - 2x_{12}x_3^3 + 30x_{12}x_3^2 - 96x_{12}x_3 + 88x_{12} \\
&\quad +x_3^4 - 24x_3^2 + 64x_3 - 48\Big) \\
&+ 4(\Delta y_{12})^4 y_3^2 + 2(\Delta y_{12})^4 y_3(3x_{12} - 1) \\
&+ (\Delta y_{12})^4(3x_{12}^2 + 2x_{12}x_3 - 6x_{12} + 2x_3^2 - 6x_3 + 4) \\
&- 8(\Delta y_{12})^2 y_3^4 \\
&+ 4(\Delta y_{12})^2 y_3^3(x_{12}x_3 - 4x_{12} + 2x_3^2 + 2x_3 - 7) \\
&+ 4(\Delta y_{12})^2 y_3^2 \\
&\times \Big(2x_{12}^2x_3 - 2x_{12}^2 + 3x_{12}x_3^2 - 4x_{12}x_3 - 7x_{12} \\
&\quad -9x_3^2 - 3x_3 + 20\Big) \\
&+ 2(\Delta y_{12})^2 y_3 \\
&\times \Big(2x_{12}^3x_3 - 2x_{12}^3 + 2x_{12}^2x_3^2 - 10x_{12}^2x_3 - 7x_{12}^2 \\
&\quad -20x_{12}x_3^2 - 4x_{12}x_3 + 48x_{12} + 10x_3^2 + 32x_3 - 52\Big) \\
&+ (\Delta y_{12})^2 \\
&\times \Big(x_{12}^4 - 14x_{12}^3 - 12x_{12}^2x_3^2 - 10x_{12}^2x_3 + 56x_{12}^2 \\
&\quad -8x_{12}x_3^3 + 36x_{12}x_3^2 + 32x_{12}x_3 - 88x_{12} - 4x_3^4 \\
&\quad +20x_3^3 - 32x_3^2 - 24x_3 + 48\Big) \\
&- (\Delta x_{12})^4 y_3^2 + 2(\Delta x_{12})^4 y_3(-x_{12} - x_3 + 2) \\
&+ (\Delta x_{12})^4(-x_{12}^2 - 2x_{12}x_3 + 4x_{12} - x_3^2 + 4x_3 - 4) \\
&+ 7(\Delta x_{12})^2 y_3^4 + 2(\Delta x_{12})^2 y_3^3(8x_{12} + 10x_3 - 19) \\
&+ 2(\Delta x_{12})^2 y_3^2 \\
&\times (6x_{12}^2 + 20x_{12}x_3 - 33x_{12} + 11x_3^2 - 43x_3 + 40) \\
&+ 2(\Delta x_{12})^2 y_3 \\
&\times \Big(2x_{12}^3 + 16x_{12}^2x_3 - 21x_{12}^2 + 20x_{12}x_3^2 - 70x_{12}x_3 \\
&\quad +56x_{12} + 6x_3^3 - 37x_3^2 + 72x_3 - 44\Big) \\
&+ (\Delta x_{12})^2\Big(x_{12}^4 + 12x_{12}^3x_3 - 14x_{12}^3 + 24x_{12}^2x_3^2 - 78x_{12}^2x_3 \\
&\quad +56x_{12}^2 + 16x_{12}x_3^3 - 90x_{12}x_3^2 + 160x_{12}x_3 \\
&\quad -88x_{12} + 3x_3^4 - 26x_3^3 + 80x_3^2 - 104x_3 + 48\Big) \\
&+ 4y_3^6 + 2y_3^5(-2x_{12}x_3 + 5x_{12} - 4x_3^2 - 4x_3 + 15) \\
&+ y_3^4\Big(-16x_{12}^2x_3 + 9x_{12}^2 - 36x_{12}x_3^2 + 38x_{12}x_3 + 50x_{12} \\
&\quad -16x_3^3 + 82x_3^2 - 14x_3 - 84\Big) \\
&+ 2y_3^3\Big(-12x_{12}^3x_3 + 2x_{12}^3 - 30x_{12}^2x_3^2 + 56x_{12}^2x_3 + 15x_{12}^2 \\
&\quad -22x_{12}x_3^3 + 126x_{12}x_3^2 - 68x_{12}x_3 - 64x_{12} - 4x_3^4 \\
&\quad +52x_3^3 - 126x_3^2 + 24x_3 + 52\Big) \\
&+ y_3^2\Big(-16x_{12}^4x_3 + x_{12}^4 - 44x_{12}^3x_3^2 + 104x_{12}^3x_3 + 10x_{12}^3 \\
&\quad -40x_{12}^2x_3^3 + 298x_{12}^2x_3^2 - 250x_{12}^2x_3 - 64x_{12}^2 \\
&\quad -12x_{12}x_3^4 + 228x_{12}x_3^3 - 644x_{12}x_3^2 + 288x_{12}x_3 \\
&\quad +104x_{12} + 40x_3^4 - 260x_3^3 + 456x_3^2 - 152x_3 - 48\Big) \\
&+ 2y_3x_3\Big(-2x_{12}^5 - 6x_{12}^4x_3 + 19x_{12}^4 - 6x_{12}^3x_3^2 + 66x_{12}^3x_3 \\
&\quad -74x_{12}^3 - 2x_{12}^2x_3^3 + 68x_{12}^2x_3^2 - 227x_{12}^2x_3 \\
&\quad +144x_{12}^2 + 21x_{12}x_3^3 - 156x_{12}x_3^2 + 304x_{12}x_3 \\
&\quad -136x_{12} - 17x_3^3 + 88x_3^2 - 132x_3 + 48\Big) \\
&+ x_3^2\Big(7x_{12}^4 + 16x_{12}^3x_3 - 46x_{12}^3 + 13x_{12}^2x_3^2 - 78x_{12}^2x_3 \\
&\quad +112x_{12}^2 + 6x_{12}x_3^3 - 46x_{12}x_3^2 + 128x_{12}x_3 \\
&\quad -120x_{12} + 2x_3^4 - 14x_3^3 + 44x_3^2 - 72x_3 + 48\Big)\Big\},
\end{aligned}
$$

$$
\begin{aligned}
f_{12}^1 = \frac{1}{2}\Big\{ &- 8(\Delta x_{12})^3\Delta y_{12} y_3 \\
&+ 4(\Delta x_{12})^3\Delta y_{12}(-x_{12} - x_3 + 2) \\
&+ 2(\Delta x_{12})^2(\Delta y_{12})^2 y_3(x_3 + 7) \\
&+ (\Delta x_{12})^2(\Delta y_{12})^2(2x_{12}x_3 + 4x_{12} - 2x_3 - 9) \\
&- 6\Delta x_{12}(\Delta y_{12})^3 y_3 + 2\Delta x_{12}(\Delta y_{12})^3(x_3 + 2) \\
&- 2\Delta x_{12}\Delta y_{12} y_3^3(2x_3 + 3) \\
&+ 2\Delta x_{12}\Delta y_{12} y_3^2(-4x_{12}x_3 - 2x_{12} - 2x_3^2 + 7x_3 - 10) \\
&+ 2\Delta x_{12}\Delta y_{12} y_3 \\
&\times \Big(-2x_{12}^2x_3 - 3x_{12}^2 - 2x_{12}x_3^2 + 2x_{12}x_3 + 2x_{12} \\
&\quad -x_3^2 + 8x_3\Big) \\
&+ 2\Delta x_{12}\Delta y_{12} \\
&\times \Big(-2x_{12}^3 + x_{12}^2x_3 + 8x_{12}^2 + 4x_{12}x_3^2 - 2x_{12}x_3 - 12x_{12} \\
&\quad +x_3^3 - 2x_3^2 - 4x_3 + 8\Big) \\
&- (\Delta y_{12})^4(x_{12} + 1) + 8(\Delta y_{12})^2 y_3^3
\end{aligned}
\tag{34}
$$

$$
\begin{aligned}
&+ 2(\Delta y_{12})^2 y_3^2(-x_{12}x_3 + 9x_{12} + 2x_3 + 5) \\
&+ 4(\Delta y_{12})^2 y_3(-x_{12}^2 x_3 + 2x_{12}^2 + 2x_{12}x_3 - 2x_{12} - 6x_3) \\
&+ (\Delta y_{12})^2\Big(- 2x_{12}^3 x_3 + 4x_{12}^3 + 6x_{12}^2 x_3 - 15x_{12}^2 \\
&\quad -6x_{12}x_3^2 + 16x_{12} - 4x_3^3 + 18x_3^2 - 8x_3 - 4\Big) \\
&+ (\Delta x_{12})^4 y_3 + (\Delta x_{12})^4(x_{12} + x_3 - 2) \\
&+ 2(\Delta x_{12})^2 y_3^3(-x_3 - 8) \\
&+ (\Delta x_{12})^2 y_3^2(-6x_{12}x_3 - 22x_{12} - 4x_3^2 + 4x_3 + 27) \\
&+ 2(\Delta x_{12})^2 y_3 \\
&\times \Big(- 3x_{12}^2 x_3 - 3x_{12}^2 - 4x_{12}x_3^2 + 4x_{12}x_3 + 11x_{12} \\
&\quad -x_3^3 + 6x_3^2 - 3x_3 - 8\Big) \\
&+ (\Delta x_{12})^2 \\
&\times \Big(- 2x_{12}^3 x_3 - 4x_{12}^2 x_3^2 + 10x_{12}^2 x_3 - x_{12}^2 - 2x_{12}x_3^3 \\
&\quad +18x_{12}x_3^2 - 30x_{12}x_3 + 8x_{12} \\
&\quad +8x_3^3 - 33x_3^2 + 40x_3 - 12\Big) \\
&- 8y_3^5 + y_3^4(6x_{12}x_3 - 21x_{12} + 8x_3^2 + 4x_3 - 41) \\
&+ 2y_3^3\Big(10x_{12}^2 x_3 - 9x_{12}^2 + 14x_{12}x_3^2 - 24x_{12}x_3 - 24x_{12} \\
&\quad +4x_3^3 - 24x_3^2 + 12x_3 + 44\Big) \\
&+ y_3^2\Big(24x_{12}^3 x_3 - 6x_{12}^3 + 36x_{12}^2 x_3^2 - 88x_{12}^2 x_3 - 19x_{12}^2 \\
&\quad +14x_{12}x_3^3 - 94x_{12}x_3^2 \\
&\quad +56x_{12}x_3 + 112x_{12} - 16x_3^3 + 50x_3^2 + 32x_3 - 100\Big) \\
&+ y_3\Big(12x_{12}^4 x_3 - x_{12}^4 + 20x_{12}^3 x_3^2 - 56x_{12}^3 x_3 - 10x_{12}^3 \\
&\quad +8x_{12}^2 x_3^3 - 86x_{12}^2 x_3^2 + 82x_{12}^2 x_3 \\
&\quad +64x_{12}^2 - 32x_{12}x_3^3 + 152x_{12}x_3^2 - 56x_{12}x_3 \\
&\quad -104x_{12} + 40x_3^3 - 120x_3^2 + 40x_3 + 48\Big) \\
&+ x_3\Big(2x_{12}^5 + 4x_{12}^4 x_3 - 19x_{12}^4 + 2x_{12}^3 x_3^2 - 34x_{12}^3 x_3 \\
&\quad +74x_{12}^3 - 8x_{12}^2 x_3^2 + 97x_{12}^2 x_3 - 144x_{12}^2 \\
&\quad +11x_{12}x_3^3 - 8x_{12}x_3^2 - 104x_{12}x_3 + 136x_{12} + 4x_3^4 \\
&\quad -25x_3^3 + 32x_3^2 + 28x_3 - 48\Big)\Big\},
\end{aligned}
$$

$$
\begin{aligned}
f_{12}^2 = \frac{1}{4}\Big\{ &- 4(\Delta x_{12})^3 \Delta y_{12} - 4(\Delta x_{12})^2 (\Delta y_{12})^2 \qquad (35) \\
&+ 4\Delta x_{12}(\Delta y_{12})^3 + 4\Delta x_{12}\Delta y_{12} y_3^2(x_3 - 2) \\
&+ 4\Delta x_{12}\Delta y_{12} y_3(x_{12}x_3 - 2x_{12} - 6x_3 + 8) \\
&+ 4\Delta x_{12}\Delta y_{12}(3x_{12}^2 - x_{12}x_3 - x_{12} + 4x_3 - 4) \\
&- 8(\Delta y_{12})^2 y_3^2 - 12(\Delta y_{12})^2 y_3(2x_{12} + 1) \\
&+ 4(\Delta y_{12})^2(-2x_{12}^2 + x_{12} - x_3^2 + 5x_3) + 3(\Delta x_{12})^4 \\
&+ 2(\Delta x_{12})^2 y_3^2(4x_3 + 23) \\
&+ 2(\Delta x_{12})^2 y_3(8x_{12}x_3 + 20x_{12} + 4x_3^2 - 6x_3 - 17) \\
&+ 2(\Delta x_{12})^2 \\
&\times \Big(4x_{12}^2 x_3 + 4x_{12}x_3^2 + 4x_{12}x_3 - 9x_{12} + 5x_3^2 \\
&\quad -27x_3 + 16\Big) \\
&+ 24y_3^4 + 4y_3^3(-3x_{12}x_3 + 17x_{12} - 2x_3^2 + 2x_3 + 21) \\
&+ 2y_3^2\Big(- 16x_{12}^2 x_3 + 27x_{12}^2 - 10x_{12}x_3^2 \\
&\quad +46x_{12}x_3 + 22x_{12} + 22x_3^2 - 50x_3 - 52\Big) \\
&+ 2y_3\Big(- 14x_{12}^3 x_3 + 6x_{12}^3 - 10x_{12}^2 x_3^2 + 44x_{12}^2 x_3 - 7x_{12}^2 \\
&\quad +18x_{12}x_3^2 - 12x_{12}x_3 - 32x_{12} + 10x_3^2 \\
&\quad -56x_3 + 44\Big) \\
&- 8x_{12}^4 x_3 + x_{12}^4 - 8x_{12}^3 x_3^2 + 8x_{12}^3 x_3 + 10x_{12}^3 + 18x_{12}^2 x_3^2 \\
&+ 86x_{12}^2 x_3 - 64x_{12}^2 + 28x_{12}x_3^3 - 52x_{12}x_3^2 - 176x_{12}x_3 \\
&+ 104x_{12} + 12x_3^4 - 68x_3^3 + 88x_3^2 + 72x_3 - 48\Big\},
\end{aligned}
$$

$$
\begin{aligned}
f_{12}^3 = \frac{1}{2}\Big\{ &2(\Delta y_{12})^2(x_{12} + 1) \qquad (36) \\
&+ 2\Delta y_{12}\Delta x_{12}(3y_3 + 2x_{12} - x_3 - 2) \\
&- 2(\Delta x_{12})^2 y_3(x_3 + 6) \\
&+ (\Delta x_{12})^2(-2x_{12}x_3 - 6x_{12} + 8x_3 + 1) \\
&- 8y_3^3 + 2y_3^2(x_{12}x_3 - 13x_{12} - 2x_3 - 11) \\
&+ 2y_3(2x_{12}^2 x_3 - 9x_{12}^2 - 8x_{12}x_3 + 20x_3 + 4) \\
&+ 2x_{12}^3 x_3 - 2x_{12}^3 - 12x_{12}^2 x_3 + 11x_{12}^2 + 6x_{12}x_3^2 \\
&+ 24x_{12}x_3 - 16x_{12} + 4x_3^3 - 22x_3^2 + 4\Big\},
\end{aligned}
$$

$$
\begin{aligned}
f_{12}^4 = \frac{1}{4}\Big\{ &3(\Delta x_{12})^2 - 2\Delta y_{12}\Delta x_{12} + 4y_3^2 + 2y_3(9x_{12} + 7) \qquad (37) \\
&+ 9x_{12}^2 - 2x_{12}x_3 + 2x_{12} + 2x_3^2 - 14x_3 - 4\Big\},
\end{aligned}
$$

$$
f_{12}^5 = -\frac{1}{2}(x_{12} + 1), \qquad (38)
$$

where $x_{12} = x_1 + x_2$, $\Delta x_{12} = x_1 - x_2$, and $\Delta y_{12} = y_1 - y_2$. It is easy to see that the equations for f_{12}^k are symmetric under the interchange $(x_1, y_1) \leftrightarrow (x_2, y_2)$.

The expressions for the other $\mathcal{F}_{ij}(x_i, y_i, z_0)$ can be derived from the ones given above by using the Bose symmetry.

References

1. F.J. Gilman, R. Kauffman, Phys. Rev. D **36**, 2761 (1987) [Erratum D **37**, 3348 (1988)]
2. H. Leutwyler, Nucl. Phys. Proc. Suppl. **64**, 223 (1998) [hep-ph/9709408]
3. R. Kaiser, H. Leutwyler, Eur. Phys. J. C **17**, 623 (2000) [hep-ph/0007101]
4. T. Feldmann, P. Kroll, B. Stech, Phys. Rev. D **58**, 114006 (1998) [hep-ph/9802409]

5. T. Feldmann, P. Kroll, B. Stech, Phys. Lett. B **449**, 339 (1999) [hep-ph/9812269]
6. P. Ball, J.M. Frere, M. Tytgat, Phys. Lett. B **365**, 367 (1996) [hep-ph/9508359]
7. D. Atwood, A. Soni, Phys. Lett. B **405**, 150 (1997) [hep-ph/9704357]
8. W.S. Hou, B. Tseng, Phys. Rev. Lett. **80**, 434 (1998) [hep-ph/9705304]
9. A.L. Kagan, A.A. Petrov, hep-ph/9707354
10. I.E. Halperin, A. Zhitnitsky, Phys. Rev. Lett. **80**, 438 (1998) [hep-ph/9705251]
11. F. Yuan, K.T. Chao, Phys. Rev. D **56**, 2495 (1997) [hep-ph/9706294]
12. A. Datta, X.G. He, S. Pakvasa, Phys. Lett. B **419**, 369 (1998) [hep-ph/9707259]
13. M.R. Ahmady, E. Kou, A. Sugamoto, Phys. Rev. D **58**, 014015 (1998) [hep-ph/9710509]
14. I.E. Halperin, A. Zhitnitsky, Phys. Rev. D **56**, 7247 (1997) [hep-ph/9704412]
15. H.Y. Cheng, B. Tseng, Phys. Lett. B **415**, 263 (1997) [hep-ph/9707316]
16. A.S. Dighe, M. Gronau, J.L. Rosner, Phys. Rev. Lett. **79**, 4333 (1997) [hep-ph/9707521]
17. N.G. Deshpande, B. Dutta, S. Oh, Phys. Rev. D **57**, 5723 (1998) [hep-ph/9710354]
18. D. s. Du, C.S. Kim, Y. d. Yang, Phys. Lett. B **426**, 133 (1998) [hep-ph/9711428]
19. A. Ali, J. Chay, C. Greub, P. Ko, Phys. Lett. B **424**, 161 (1998) [hep-ph/9712372]
20. A. Ali, G. Kramer, C.D. Lu, Phys. Rev. D **58**, 094009 (1998) [hep-ph/9804363]
21. M. Beneke, M. Neubert, Nucl. Phys. B **651**, 225 (2003) [hep-ph/0210085]
22. A.L. Kagan, AIP Conf. Proc. **618**, 310 (2002) [hep-ph/0201313]; Y. Chen, A.L. Kagan, Univ. of Cincinnati preprint, in preparation
23. T. Muta, M.Z. Yang, Phys. Rev. D **61**, 054007 (2000) [hep-ph/9909484]
24. A. Ali, A.Y. Parkhomenko, Phys. Rev. D **65**, 074020 (2002) [hep-ph/0012212]
25. P. Kroll, K. Passek-Kumericki, Phys. Rev. D **67**, 054017 (2003) [hep-ph/0210045]
26. S.S. Agaev, N.G. Stefanis, hep-ph/0212318
27. M.V. Terentev, Sov. J. Nucl. Phys. **33**, 911 (1981) [Yad. Fiz. **33**, 1692 (1981)]
28. T. Ohrndorf, Nucl. Phys. B **186**, 153 (1981)
29. M.A. Shifman, M.I. Vysotsky, Nucl. Phys. B **186**, 475 (1981)
30. V.N. Baier, A.G. Grozin, Nucl. Phys. B **192**, 476 (1981)
31. M.V. Terentev, JETP Lett. **33**, 67 (1981) [Pisma Zh. Eksp. Teor. Fiz. **33**, 71 (1981)]
32. A.V. Belitsky, D. Muller, Nucl. Phys. B **537**, 397 (1999) [hep-ph/9804379]
33. J. Gronberg et al. [CLEO Collaboration], Phys. Rev. D **57**, 33 (1998) [hep-ex/9707031]
34. M. Acciarri et al. [L3 Collaboration], Phys. Lett. B **418**, 399 (1998)
35. M. Artuso et al. [CLEO Collaboration], Phys. Rev. D **67**, 052003 (2003) [hep-ex/0211029]
36. A. Ali, A.Y. Parkhomenko, The $\eta' g^* g^*$ Vertex Including the η'-Meson Mass, CERN-TH/2003-063 [hep-ph/0307092]
37. P.B. Mackenzie, G.P. Lepage, Phys. Rev. Lett. **47**, 1244 (1981)
38. F. James, M. Roos, Comput. Phys. Commun. **10**, 343 (1975)
39. T. Feldmann, Int. J. Mod. Phys. A **15**, 159 (2000) [hep-ph/9907491]
40. T. Feldmann, P. Kroll, Phys. Scripta T **99**, 13 (2002) [hep-ph/0201044]